Theor Chem Acc (2006) 116: 390–397
DOI 10.1007/s00214-006-0081-9

REGULAR ARTICLE

M. E. Alikhani · S. Shaik

A topological study of the ferromagnetic "no-pair bonding" in maximum-spin lithium clusters: $^{n+1}Li_n$ (n=2–6)

Received: 14 October 2004 / Accepted: 5 March 2005 / Published online: 17 February 2006

Abstract The nature of the bonding between lithium atoms, in low-spin and maximum-spin Li_n(n=2–6) clusters, was investigated using the topological electron localization function (ELF) approach. The maximum-spin clusters are especially intriguing since their bonding is sustained without having even a single electron pair! Hence this type of bonding had been called "no-pair ferromagnetic-bonding" [Danovich, Wu, Shaik J Am Chem Soc 121:3165 (1999); Glokhovtsev, Schleyer Isr J Chem 33:455 (1993); de Visser, Danovich, Wu, Shaik J Phys Chem A 106:4961 (2002)]. The following conclusions were reached in the study: (a) In the ground state of Li_n, covalent bonding between Li atoms is accounted by the presence of the disynaptic valence basins, which exhibit a significant degree of inter-basin delocalization. (b) Except for the $^3Li_2$ case, the valence basins of all maximum-spin clusters are populated by unpaired electrons. The valence basins are located off Li–Li axis (or Li–Li–Li plane), so that their spatial distribution minimizes the mutual Pauli repulsion and screens the electrostatic repulsion between the Li cores. The inter-basin delocalization is rather high, thereby indicating that the unpaired electrons are virtually delocalized over all the valence basins. (c) The ELF analysis shows that Li atoms in the low-spin clusters are bonded by "two-center two-electron" and "three-center two-electron" bonds. (d) In the maximum-spin species, bonding is sustained by "two-center one-electron" and "three-center one-electron" bonds. The latter picture is complementary to the valence bond picture [Danovich, Wu, Shaik J Am Chem Soc 121:3165 (1999); de Visser, Danovich, Wu, Shaik J Phys Chem A 106:4961 (2002)], in which the bicentric ferromagnetic-bonding is delocalized over all the short Li–Li contacts, by the mixing of the ionic structures and other nonredundant structures into the repulsive high-spin covalent structure in which all the electrons populate the 2s atomic orbitals, i.e., the $2s_a^1 2s_b^1\ 2s_i^1 \cdots 2s_n^1$ configuration. In such a manner bonding can be sustained from "purely ferromagnetic interactions" without electron pairing.

Dedicated to Jean-Paul Malrieu, a friend and a poet-scientist

M. E. Alikhani (✉)
Laboratoire de Dynamique, Interactions et Réactivité, UMR 7075,
Université P. et M. Curie, Boîte 49, bâtiment F74, 4 Place Jussieu,
75252 Paris Cedex 05, France
E-mail: ea@spmol.jussieu.fr

S. Shaik
The Department of Organic Chemistry and the Lise Meitner-Minerva Center for Computational Quantum Chemistry,
The Hebrew University of Jerusalem, 91904 Jerusalem, Israel
E-mail: sason@yfaat.ch.huji.ac.il

1 Introduction

According to both molecular orbital (MO) and valence bond (VB) theories, singlet electron-pairing is a fundamental form of bonding in the ground state of closed-shell molecules, whereas triplet coupling is associated with a repulsive antibonding interaction. This paradigm seems, however, to breakdown as we move away from H_2 to bonding in alkali dimers and higher clusters. Thus, in contrast with the triplet $^3\Sigma_u^+$ state of H_2, the same state of Li_2 is bound, albeit by a small amount (see Ref. [1] and references therein). This small bonding energy rises however quite steeply as the high-spin $^{n+1}Li_n$ cluster increases in size, reaching 0.5 eV/atom for $^{13}Li_{12}$, despite the lack of any electron pairs between the atoms [2,3]. Accordingly, this bonding was called either "no-pair bonding" [2,3] or "ferromagnetic bonding" [1,3]. The theoretical studies further showed that the ferromagnetically bonded species assume highly symmetric geometries in which each Li atom maximizes its coordination number; these geometries are unstable in the ground state low-spin situations [3]. Such clusters are not merely theoretical curiosities, but are observed by spectroscopic techniques [4–10]. Owing to the novelty of this no-pair ferromagnetic-bonding, and its occurrence in alkali clusters, it was deemed necessary to probe the nature of this bonding by theoretical means alternative to VB or MO theories.

A VB study of the lithium dimer revealed that the dominant configuration of the singlet and triplet state wave

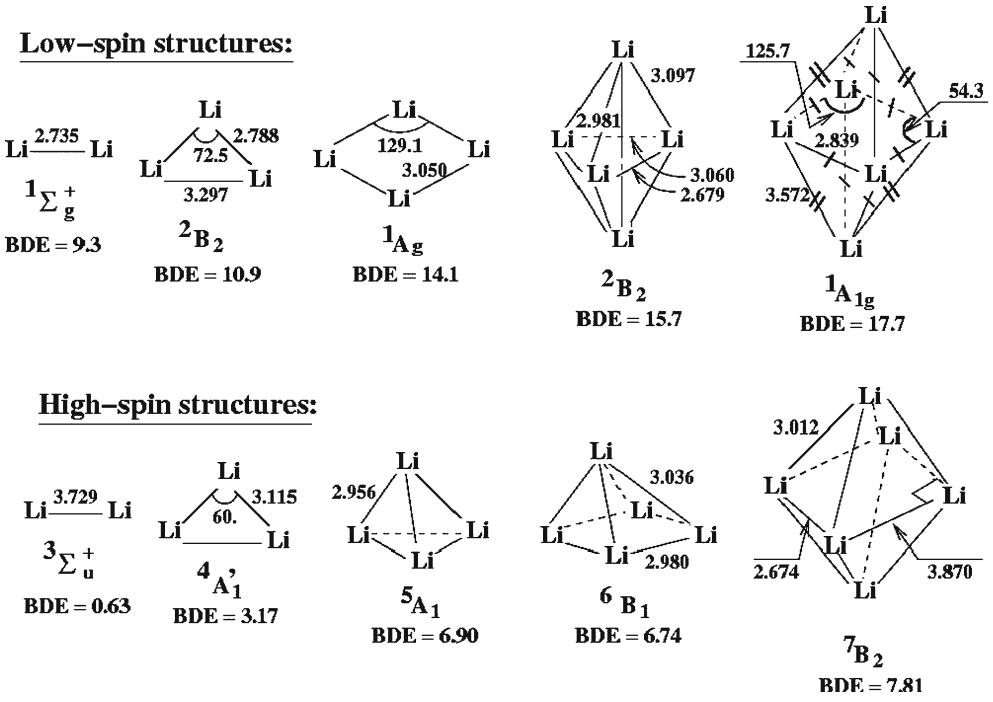

Scheme 1 Geometries of the ground states (*upper series*) and high-spin states (*lower series*) of the studied $Li_{2–6}$ clusters. Distances are given in Å and angles in degrees; *BDE* bond dissociation energy per atom (in kcal/mol), at the B3PW91/6-311G(2*d*) level

functions is the covalent structure in the appropriate spin state, $^{1,3}\Phi$. As expected, in the singlet state the covalent structure is bound and the bonding is further augmented by the mixing in of ionic structures. However, in the triplet no-pair state the covalent structure is repulsive, and the entire bonding arises from the perturbative mixing of triplet ionic structures and other nonredundant covalent structures into the principal structure. Particularly, it has been shown that the resonance stabilization of the ferromagnetic no-pair bond due to VB mixing is cumulative and increases with the coordination number of the Li atom in the cluster [1,3]. Thus, according to VB theory ferromagnetic bonding is highly delocalized among all close neighbors of a given atom in the cluster.

An alternative approach to the MO and VB methods for studying the nature of chemical bonding and its evolution is provided by the topological analysis of bonding. In this approach, the spatial distribution of the electron density is investigated in the real space of the molecule using a local function for a gradient field vector. The most popular topological analyses are the "atoms in molecules (AIM)" theory proposed by Bader [11], based on the electron density [$\rho(r)$] as the local function, and the electron localization function (ELF) analysis proposed by Silvi and Savin [12], based on the ELF of Becke and Edgecombe [13]. The ELF approach provides the spatial distribution of the electron pairing within a molecule, and thereby enables to propose a global scheme of the bonding. Accordingly, the present work investigates topological properties of the bonding between Li atoms in the low- and high-spin clusters (Li_n with n=2–6) using ELF to interrogate bonding.

2 Computational details

All calculations have been performed with the Gaussian 03 quantum chemical package [14] using density functional theory (DFT) approach. As shown previously [3], for the Li clusters, the DFT approach provides reasonable structural and bond energy results, close to those obtained at the coupled-cluster [CCSD(T)] level of theory. Thus, the DFT calculations were carried out with Becke's [15] three parameters hybrid method using the Perdew–Wang [16] gradient-corrected correlation functional (denoted as B3PW91). The standard 6-311G basis set [17–19] augmented by 2*d* polarization functions, hence 6-311G(2*d*), was used for Li. The full optimization of the studied clusters with B3PW91/6-311G(2*d*) has been performed using the point group symmetry proposed in the Refs. [20,21] for low-spin clusters and in the Ref. [22] for maximum-spin ones. The optimized geometries, at the B3PW91/6-311G(2*d*) level of theory, for the two species types are given in Scheme 1. For each molecule, the electronic state and bond dissociation energy per atom (BDE) have been also reported in Scheme 1.

The bonding characteristics of the studied species have been investigated using TopMoD package [23].

3 Topological analysis of the ELF function

3.1 A brief review of ELF

The topological description of the chemical bond proposed by Silvi and Savin [12] relies upon the gradient field analysis of

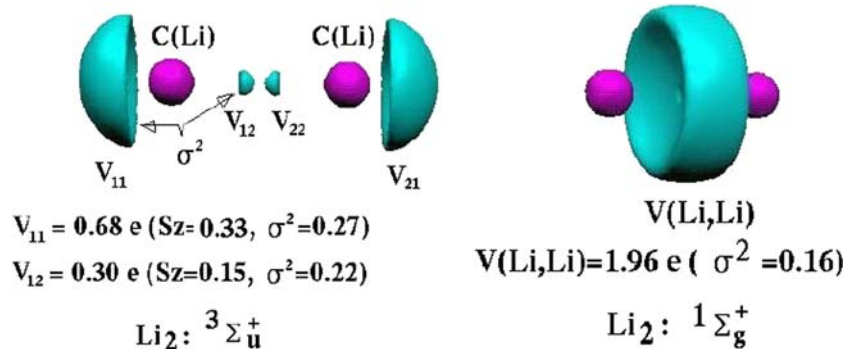

Fig. 1 Electron localization function (ELF) isosurface basins of the high- and low-spin of Li_2 dimer. Here and elsewhere, the S_z values, which appear for the high-spin states, correspond to the integrated expectation value of the spin quantum number in the basin. The valence basins are given for the ELF values η=0.89 (*left*) and 0.98 (*right*)

the ELF of Becke and Edgecombe [13]. The original expression of the ELF is given by Eq. (1) and by construction is allowed to have values in the range between $\eta = 0$ and $\eta = 1$:

$$\eta(r) = \frac{1}{1 + \left(D_\sigma / D_\sigma^0\right)^2} \tag{1}$$

Here D_σ represents the curvature of the electron pair density for electrons of identical σ spins (the Fermi hole) for the actual system, and D_σ^0 for a homogeneous electron gas with the same density as the real system. D_σ which is a positive quantity is also a measure of the excess local kinetic energy due to Pauli repulsion; it is small in regions of space where the electrons do not experience Pauli repulsion, namely either where an electron is alone or when electrons form pairs of antiparallel spins, or still, where the electrons possessing parallel spins are far from one another. The original derivation of the ELF considers the Laplacian of the Hartree–Fock conditional probability of finding a σ-spin electron at position r_2, when a first σ-spin electron is located at r_1.

$$\begin{aligned} D_\sigma &= \left[\nabla_2^2 P_{\text{cond}}^{\sigma\sigma}(1,2)\right]_{1=2} \\ &= \sum_i |\nabla \varphi_i|^2 - \frac{1}{4}\frac{\left|\nabla \rho^\sigma(1)\right|^2}{\rho^\sigma(1)} \end{aligned} \tag{2}$$

In a rigorous sense, this expression of the ELF (i.e., η), based on Eqs. (1) and (2), is valid for closed-shell systems described by a single determinant. However, acceptable results have been obtained for open-shell systems, yielding similar atomic shell populations compared to those obtained with a spin-polarized formula [24]. Therefore, most applications on radicals can be carried out with the standard ELF equation.

The topological analysis of the ELF quantity provides a partition scheme of the molecular space into basins of attractors that have clear chemical significance [25]. These basins are either core basins surrounding nuclei or valence basins. Accordingly, monosynaptic basins correspond to lone pair regions [labeled as V(X) where X is atom label] whereas disynaptic ones correspond to bicentric bonding regions [labeled as V(X, Y) where X and Y are atom labels], etc. The partition into basins allows the calculation of related properties by integration of the respective property density over a desired basin [26].

In particular, the average population for a basin, labeled Ω_A, is given as:

$$\overline{N}(\Omega_A) = \int_{\Omega_A} \rho(r)\mathrm{d}r \tag{3}$$

A measure of delocalization [27] is provided by the quantum mechanical uncertainty, in $\overline{N}(\Omega_\alpha)$, that is represented by its variance or fluctuation σ^2 (Ω_A), defined by:

$$\sigma^2(\Omega_A) = \int_{\Omega_A} \mathrm{d}r_1 \int_{\Omega_A} \mathrm{d}r_2 \pi(r_1, r_2) + \overline{N}(\Omega_A) - [\overline{N}(\Omega_A)]^2 \tag{4}$$

where $\pi(r_1, r_2)$ is the spinless pair function [28]. Following Bader's [29] definition in the case of atomic basins (in ρ) the relative fluctuation is simply defined as:

$$\lambda(\Omega_A) = \frac{\sigma^2(\Omega_A)}{\overline{N}} \tag{5}$$

This quantity gauges the delocalization within a basin Ω_A. A value of 0.45 has been quoted before [30] to be a significant delocalization from a basin.

Topological properties of ELF also enable to construct the molecular graph, thereby providing a complete representation of the bonding in a molecule, with bonds and lone pairs and their organization around the core basins. Evolution of the number of the valence basins along the reaction pathway allows one to rationalize the formation (or breaking) of a bond (see Refs. [31–34] for a detailed discussion).

3.2 Results and discussion

The ELF isosurfaces of Li_2, in the ground state and in the no-pair triplet state, are displayed in Fig. 1. We note that the Li–Li bonding in the ground state, $^1\Sigma_g^+$, is characterized by one disynaptic basin, located in the middle of the Li–Li bond.

The population of V(Li, Li) is 1.96 e with a variance being equal to 0.16. The calculated relative fluctuation λ(0.08) is very low indicating that the valence electron pairing is mostly localized in the disynaptic V(Li, Li) valence basin. By contrast, in the triplet state, we find four attractors corresponding to four valence basins (labeled in Fig. 1 as V_{11}, V_{12}, V_{21}, and V_{22}). Here in $Li_2(^3\Sigma_u^+)$, we clearly have two monosynaptic basins (labeled as V_{11} and V_{21}, in Fig. 1), which are located on the molecular axis and point away from the Li core basins [C(Li)]. The two valence basins V_{12} and V_{22} that are located between two Li core basins and characterized by two distinct attractors should be globally considered as disynaptic basins carrying a part of unpaired electrons of the triplet state.

Figure 2 displays the corresponding molecular graphs along the Li–Li interatomic distance in the triplet state $^3\Sigma_u^+$. The total energy (in Hartree) is reported on the y axis and the Li–Li distance (in Å) on the x axis. As the Li atoms approach one another, a topological catastrophe occurs around $R \approx 4.8$ Å. To the right side of this point, the molecular graph is characterized by four attractors [two core, C(Li), and two valence, V(Li)] and the two unpaired electrons are lodged in the two monosynaptic V(Li) basins; namely the electrons are localized on the atoms and keep away from each other so as to minimize the Pauli repulsion. By contrast, to the left side of $R \approx 4.8$ Å, each of the V(Li) basins splits into two basins producing four valence attractors, now indicating that part of the electron density of the triplet participates in bonding of the two cores.

Table 1 reports the evolution of the geometrical parameters and of the valence basin populations of the $^3Li_2$ triplet state, for the region of ferromagnetic bonding in Fig. 2 (corresponding to the left of $R \approx 4.8$ Å). We note that the distances r_1 and r_2 slightly increase when the Li–Li distance [R(Li–Li)] decreases. These changes lead to the reduction of the r_3 distance, so that the difference between two r_1 and r_2 distances is minimized (0.093 Å) and the quadrupole moment is maximized ($\Theta_{ZZ} = -20.4\,D$ Å) at the equilibrium structure. As further shown in Table 1, the populations of V_{12} and V_{22} (the two are identical by symmetry) increase and reach a maximum value (0.30 e), as the internuclear distance decreases. At the equilibrium geometry [R(Li–Li)=3.729 Å] the population of V_{11} (or the identical by symmetry V_{21}) is nearly twice that of V_{12} (or V_{22}), and the delocalization between the latter basins is high, involving most of the respective population (λ=0.7). This indicates significant delocalization of the valence basins by charge transfer from one Li to the other, in accord with the results of the VB study [1,3]. In addition, the split of Li valence basin around of each Li core could be understood as an outcome of the screening of the electrostatic repulsion between two Li cores (Li^+), which helps creating a bounded no-pair state.

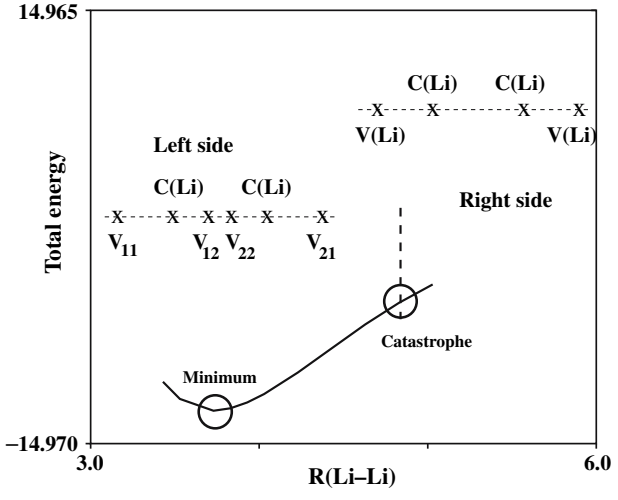

Fig. 2 Topological evolution of the $Li_2^3\Sigma_u^+$ state along the Li–Li distance

Table 1 Evolution of the geometrical parameters (in Å) and of the valence basin populations (in e) as a function of the Li–Li distance, in the left side of Fig. 2

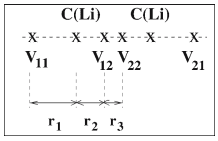

r_1	r_2	r_3	R(Li–Li)	V_{11}	V_{12}
1.566	1.457	1.703	4.629	0.88	0.10
1.567	1.459	1.510	4.429	0.80	0.18
1.568	1.463	1.304	4.229	0.73	0.25
1.570	1.475	1.078	4.029	0.71	0.27
1.571	1.485	0.958	3.929	0.70	0.28
1.572	1.522	0.685	3.729	0.68	0.30

As shown in Fig. 3, the Li trimer has a C_{2v} symmetry in the low-spin state ($^2B_2$) and a D_{3h} symmetry in the high-spin state ($^4A_1'$). In both ground and excited states, three valence basins were found in the valence regions. In the ground state, one of the three valence basins is a disynaptic one and its attractor is located in the middle of Li–Li bond. The population of this basin is 1.15 e with an integrated spin density equal to 0.0 indicating that we have "a half of an electron-pair" in this basin. The variance of the disynaptic basin population is 0.57 (λ=0.5). Analysis of the covariance shows that the cross-exchange between the disynaptic and monosynaptic basins is rather high (48% of the disynaptic basin populations), indicating a strong symmetric delocalization with two monosynaptic basins. These monosynaptic basins are symmetrically located on the sides of the Li atom that lies on the C_{2v} axis and contain 1.8 e. As shown in Fig. 4, for $^2B_2$, each of these two monosynaptic basins is characterized by one attractor that lies off the Li–Li axis (with an angle close to 99°) and close to the Li atom on the C_{2v} axis. The disynaptic attractor for $^2B_2$ is a little off the Li–Li axis (162°), thus minimizing the Pauli repulsion between the electron densities in the valence basins. The integrated spin density over each of the two monosynaptic basins is calculated to be 0.27 e (Fig. 3). The symmetric distribution of the unpaired electron on the Li atoms is consistent with the structural symmetry of the ground state trimer ($^2B_2$).

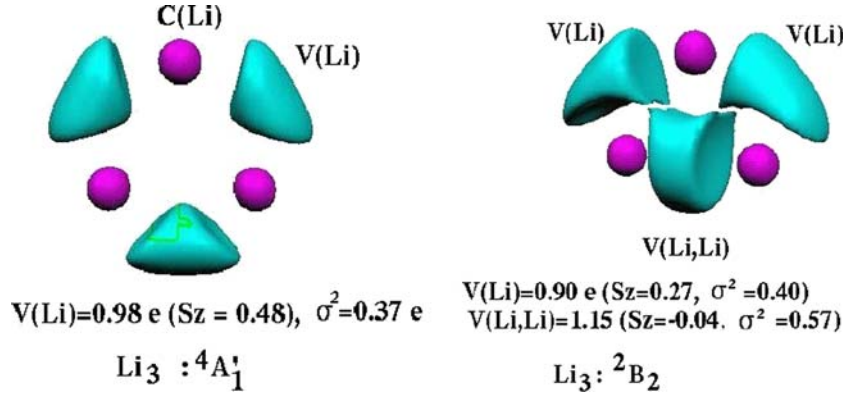

Fig. 3 ELF isosurface basins of the high- and low-spin states of the Li_3 trimer. The valence basins are given for the ELF values η=0.88 (*left*) and 0.98 (*right*)

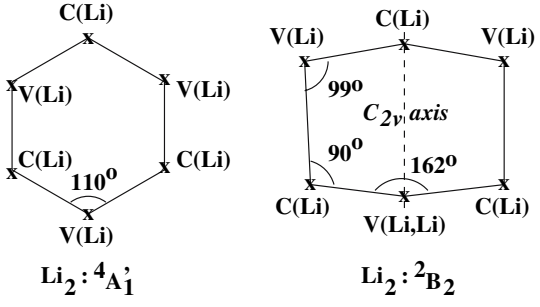

Fig. 4 Molecular graphs of Li_3 clusters in the high- and low-spin states

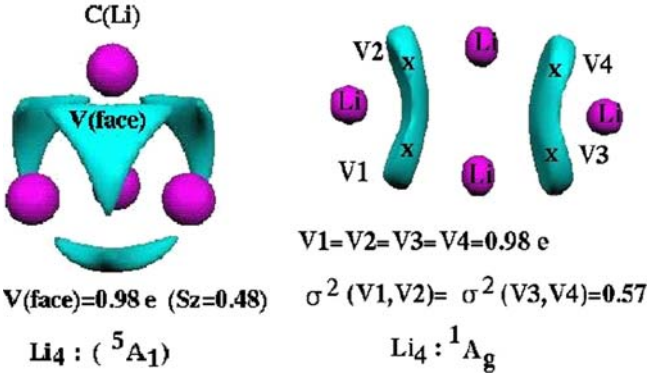

Fig. 5 ELF isosurface basins of the high- and low-spin of Li_4 tetramer. The valence basins are given for the ELF values η=0.77 (*left*) and 0.99 (*right*)

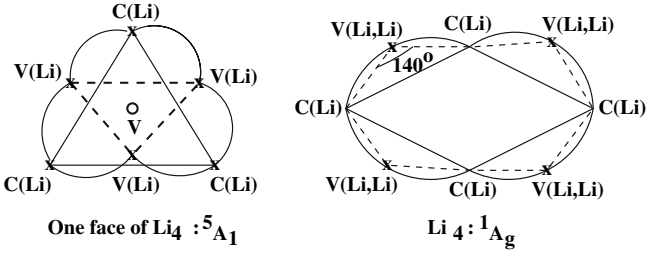

Fig. 6 Molecular graphs of Li_4 complexes

Consider now the high-spin structure of Li_3 displayed in Fig. 3. Here, three unpaired electrons are located in three valence basins. Attractors corresponding to each basin are symmetrically located outwardly off the Li–Li axis with $\angle$ (Li–Attractor–Li)$\approx$110° (see Fig. 4). The variance calculated for the population of each valence basin results in an important symmetric delocalization between three valence basins (with the cross- exchange being ca. 40%). In addition, these valence basins serve to minimize the electrostatic repulsion between each $Li^+ - Li^+$ pair [C(Li)–C(Li)]. Thus, the ELF picture describes a highly delocalized electronic structure, much as deduced from the VB analysis [1,3] and identical to the GVB results [35]. In the VB model [1,3], this delocalization is imparted on the quartet spin covalent structure primarily by mixing of the triplet charge transfer structures, where an electron is shifted from the 2*s* orbital of one Li to any one of the 2*p* orbitals of the other Li.

The singlet ground state of Li_4 has a planar rhomboidal structure (D_{2h} group; see Scheme 1). The ELF analysis, in Fig. 5, reveals that the bonding in this cluster could be considered as four half-pair bonds on the edges of the rhombus. As shown in Fig. 6, four attractors related to four disynaptic basins are found in the molecular plane of $Li_4(^1A_g)$, with an angle of around 140° that reveals the Pauli repulsion between the electron densities in the valence basins. It is interesting to note that there is a saddle point for each pair of the disynaptic basins (denoted as V1–V2 and V3–V4, in Fig. 5) with a high ELF value (0.944), very close to the ELF value of each attractor (0.996). Therefore, in accord with previous theoretical work [35], one may consider each pair of the disynaptic basins as a trisynaptic basin. In other words, the electrons are localized within the centers of the two triangles in $Li_4(^1A_g)$ thereby forming two three-center two-electron (3c-2e) bonds. The population of each basin presents a high delocalization (σ^2=0.57 and λ=0.58). This is a perfectly delocalized electronic structure in the sense of VB theory [36–38]. For a VB description of Li clusters, see [32].

There are also four valence basins in the high-spin tetramer (in T_d symmetry; see Scheme 1). As displayed in Fig. 5, each of the four valence basins is characterized by three

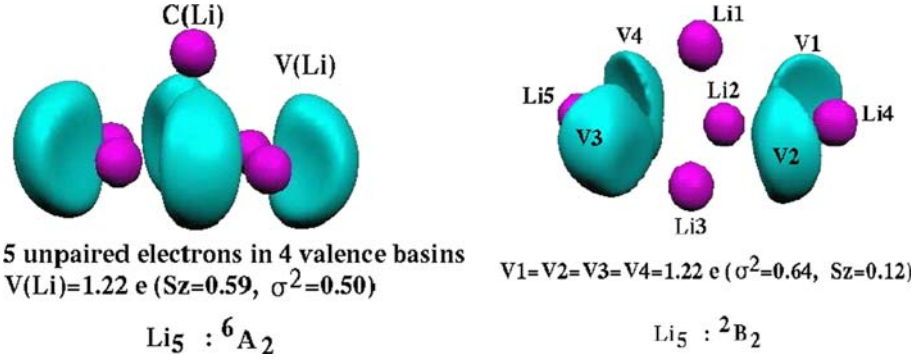

Fig. 7 ELF isosurface basins of the high- and low-spin of Li_5 pentamer. The valence basins are given for the ELF values η=0.80 (*left*) and 0.987 (*right*)

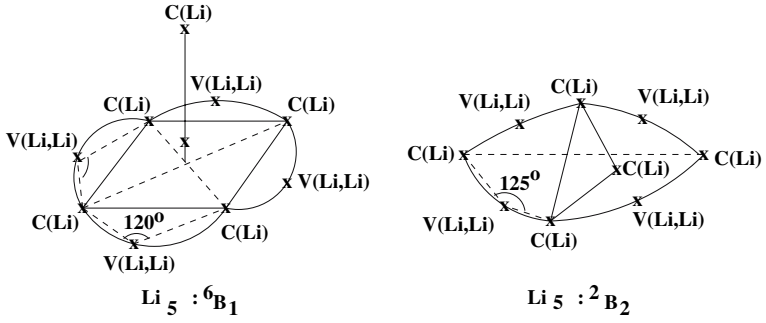

Fig. 8 Molecular graphs of Li_5 complexes

attractors for each face of $Li_4(^5A_1)$. Every C(Li)–C(Li) pair is connected by one of the three attractors. We note that the set of three attractors (of index zero) could be represented by one saddle point of index 2. This means that the electrostatic repulsion between three Li cores of each face of the molecule is minimized due to the valence basin in the saddle point, and at the same time, the Pauli repulsion between four valence basins is minimized by distributing these basins on the different faces. Therefore, each valence basin is actually a trisynaptic basin corresponding to three-center one-electron (3c-1e) bonding. As can be seen, each basin carries mostly one unpaired electron (S_z=0.48) with a strong delocalization with two other basins ($\lambda \approx 0.74$ and a large cross-exchange value). Thus, once again, we find a complementary description to the VB analysis, in which the ferromagnetic no-pair bonding is due to significant delocalization effected by the mixing of the various ionic structures into the maximal spin covalent structure, which by itself is repulsive [1,3].

The ELF isosurfaces for the Li_5 are presented in Fig. 7; the geometries of the ground- and high-spin states are displayed in Scheme 1. The ground state of the cluster ($^2B_2$) has a bipyramidal structure in the C_{2v} symmetry. The bipyramid's base is shown in Fig. 7 by the Li1, Li2, and Li3 set. There are four valence basins containing 1.22 e per basin. The delocalization between each pair of valence basins located in each pyramid is calculated to be high (σ^2=0.64 and λ=0.52). The unpaired electron density is delocalized over four valence basins (S_z=0.12 per basin). As shown in Fig. 8, the ∠(C(Li)–Attractor– C(Li)) value is calculated to be 125°. We note that the value of this angle decreases when the cluster size increases from 3 to 5, indicating the increase of the Pauli repulsion between the valence basins.

The maximum-spin cluster ($^6B_1$) has a pyramidal structure in the C_{4v} symmetry (see Scheme 1). As displayed in Fig. 7, this no-pair state has five unpaired electrons that reside in four valence basins. The molecular graph of this cluster is illustrated in Fig. 8. Four attractors corresponding to the four valence basins are located in the plane of the four Li cores, in the base of the pyramid, so that the angle ∠(Li–Attractor–Li) ≈120° (see Fig. 8). Each valence basin is shared between two Li cores, thus forming a local bicentric bonding interaction. In addition, the five unpaired electrons are symmetrically distributed within the four valence basins with an integrated spin density slightly larger than 0.5. The variance of the population of each basin indicates a moderate symmetric delocalization between four valence basins (σ^2=0.50, λ=0.41, and cross-exchange of 30%). By analogy to the VB picture [1,3], this bonding picture corresponds to bicentric ferromagnetic-bonds that fluctuate between the various Li–Li linkages. As such, the electrostatic repulsions between two neighboring Li^+ cores (in the base of the pyramid) is overcome by the presence of a valence basin, while the fifth Li^+, on the top of the pyramid is attracted by the four valence basins of the pyramid base.

As seen in Scheme 1, the Li hexamer has D_{4h} symmetry in the ground state ($^1A_{1g}$) and a C_{2v} symmetry in the no-pair high-spin state ($^7B_2$); in fact the structure of the latter state is a distorted octahedron. In the singlet ground state of Li_6,

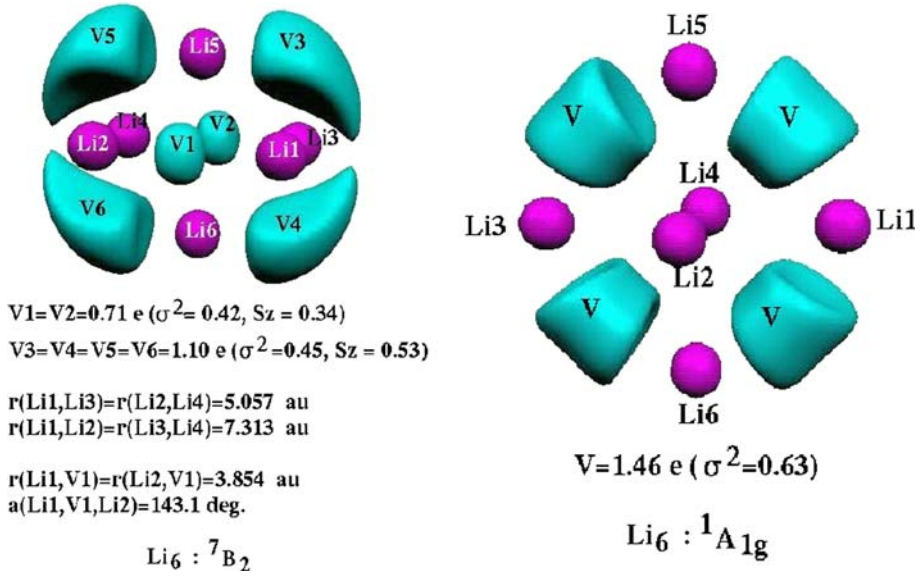

Fig. 9 ELF isosurface basins of the high- and low-spin of Li_6 hexamer. The valence basins are given for the ELF values η=0.57 (*left*) and 0.98 (*right*)

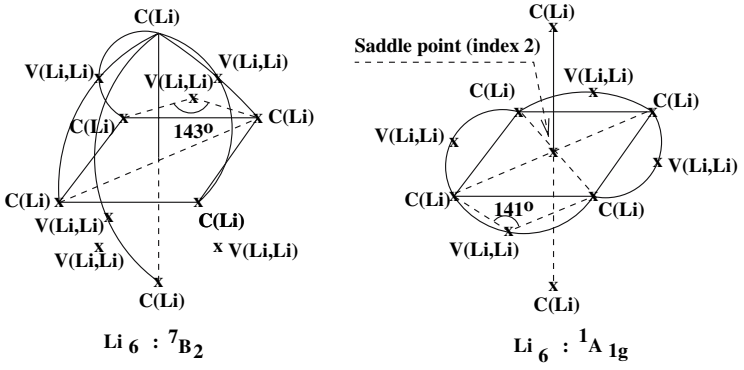

Fig. 10 Molecular graphs of Li_6 complexes

the bonding is characterized by four disynaptic basins corresponding to four attractors located between four Li atoms (see Fig. 9). The valence basins are equally populated and the delocalization between them is found to be of medium range (σ^2=0.63 and λ=0.43). From the molecular graph (Fig. 10), one can see that the attractors in the singlet structure are located in the plane of the pyramid's base, so that two apical Li^+ cores maintain an attractive interaction with the four valence basins; the latter can be represented by a central critical point (saddle point of index 2). The value of the ∠(Li– Attractor–Li) angle is around of 141°, larger than that of Li_5. The latter change is due to the larger size of Li_6 compared with Li_5.

As shown in Fig. 9, in the high-spin structure, $^7Li_6$, the six unpaired electrons are asymmetrically distributed in six valence basins (labeled as V1, V2, V3, V4, V5, and V6 in Fig. 9). The six corresponding attractors, two equatorial attractors and four facial ones, are out of planes (see Fig. 10). We note that the angle between an attractor and two Li cores is again larger than the value obtained for the smaller clusters (∠(Li–Attractor–Li)≈143°). The equatorial valence basins are less populated than the facial ones (0.71 vs. 1.10 e). However, there is a strong delocalization between six valence basins. Once again we see a corollary between the VB [1, 3] and ELF descriptions in terms of extensively delocalized ferromagnetic bonding.

4 Conclusions

The ELF analysis of the small cluster of Li_n (n=2–6), in both the ground states and the corresponding no-pair maximum-spin states, reveals the following bonding features:

(a) In the ground state of Li_n, there is covalent bonding between Li atoms and the clusters exhibit 2c-2e and 3c-2e bonding features. This bonding is accounted by the presence of the disynaptic and trisynaptic valence basins. The delocalization between valence basins is rather high, particularly in the species with a doublet-spin ground state. Except for the Li_2 case, in all other clusters, the attractors corresponding to the disynaptic basins are always located slightly out of the Li–Li axis (125–162°) satisfying the Pauli repulsion,

while attractors related to the monosynaptic basins are out of Li–Li axis and close to one of the Li atoms. (b) In the maximum-spin clusters, the valence basins are populated by unpaired electrons, thus having 2c-1e and 3c-1e bonds. The basins are located off Li–Li axis (or Li–Li–Li plane), except for the Li_2 case, so that their spatial distribution minimizes both the mutual Pauli repulsion of the electrons as well as of the electrostatic repulsion between the Li cores. The symmetry of the valence attractors accords with the structural symmetry of the high-spin cluster at the equilibrium geometry. The ∠(Li–Attractor–Li) angle increases when the cluster size increases. The inter-basin delocalization of the valence basins is rather high indicating that the unpaired electrons are virtually delocalized over the valence basins.

In summary, ELF and VB lead to similar but complementary bonding pictures of no-pair ferromagnetic-bonding. In the ELF description, the bonding picture is highly delocalized with fluctuation between the basins. In the VB description [1,3] the bicentric ferromagnetic-bonding is delocalized over all the short Li– Li contacts, by the mixing of the ionic structures (locally triplet ionics) and other nonredundant structures into the repulsive high-spin covalent structure in which all the electrons populate the 2*s* atomic orbitals, i.e., the $2s_a^1 2s_b^1 \cdots 2s_i^1 \cdots 2s_n^1$ configuration. As a complementary aspect, VB theory adds the energy aspect and shows that the binding energy of the no-pair cluster can be estimated simply by summing up all the close neighbor interactions of a given atom due to the mixing of the charge transfer and other nonredundant maximum-spin structures into the fundamental repulsive covalent structure, $2s_a^1 2s_b^1 \cdots 2s_i^1 \cdots 2s_n^1$. In such a manner bonding can be sustained from "purely ferromagnetic interactions".

References

1. Danovich D, Wu W, Shaik S (1999) J Am Chem Soc 121:3165
2. Glokhovtsev MN, Schleyer PVR (1993) Isr J Chem 33:455
3. de Visser SP, Danovich D, Wu W, Shaik S (2002) J Phys Chem A 106:4961
4. Higgins J, Callegari C, Reho J, Stienkemeier F, Ernst WE, Lehmann KK, Gutowski M, Scoles G (1996) Science 273:629
5. Higgins J, Ernst WE, Callegari C, Reho J, Lehmann KK, Scoles G (1996) Phys Rev Lett 77:4532
6. Higgins J, Callegari C, Reho J, Stienkemeier F, Ernst WE, Gutowski M, Scoles G (1998) J Phys Chem A 102:4952
7. Fiortti A, Comparat D, Crubelier A, Dulieu D, Mansou-Seeuws F, Pillet P (1998) Phys Rev Lett 80:4402
8. Higgins J, Hollebeek T, Reho J, Ho T-S, Lehmann KK, Rabitz H, Scoles G, Gutowski M (2000) J Chem Phys 112:5751
9. Reho JH, Higgins J, Nooijen M, Lehmann KK, Scoles G (2001) J Chem Phys 115:10265
10. Brühl FR, Miron RA, Ernst WE (2001) J Chem Phys 115:10275
11. Bader RFW (1994) Atoms in molecules: a quantum theory. Oxford University Press, Oxford
12. Silvi B, Savin A (1994) Nature 371:683
13. Becke AD, Edgecombe KE (1990) J Chem Phys 92:5397
14. Frisch MJ, Trucks GW, Schlegel HB, Scuseria GE, Robb MA, Cheeseman JR, Montgomery, Jr. JA, Vreven T, Kudin KN, Burant JC, Millam JM, Iyengar SS, Tomasi J, Barone V, Mennucci B, Cossi M, Scalmani G, Rega N, Petersson GA, Nakatsuji H, Hada M, Ehara M, Toyota K, Fukuda R, Hasegawa J, Ishida M, Nakajima T, Honda Y, Kitao O, Nakai H, Klene M, Li X, Knox JE, Hratchian HP, Cross JB, Adamo C, Jaramillo J, Gomperts R, Stratmann RE, Yazyev O, Austin AJ, Cammi R, Pomelli C, Ochterski JW, Ayala PY, Morokuma K, Voth GA, Salvador P, Dannenberg JJ, Zakrzewski VG, Dapprich S, Daniels AD, Strain MC, Farkas O, Malick DK, Rabuck AD, Raghavachari K, Foresman JB, Ortiz JV, Cui Q, Baboul AG, Clifford S, Cioslowski J, Stefanov BB, Liu G, Liashenko A, Piskorz P, Komaromi I, Martin RL, Fox DJ, Keith T, Al-Laham MA, Peng CY, Nanayakkara A, Challacombe M, Gill PMW, Johnson B, Chen W, Wong MW, Gonzalez C, Pople JA (2003) Gaussian 2003, Revision B.02. Gaussian, Inc., Pittsburgh PA
15. Becke AD (1993) J Chem Phys 98:5648
16. Perdew JP, Wang Y (1992) Phys Rev B 45:13244
17. Krishnan R, Binkley JS, Seeger R, Pople JA (1980) J Chem Phys 72:650
18. Clark T, Chandrasekhar J, Spitznagel GW, Schleyer PVR (1983) J Comp Chem 4:294
19. Frisch MJ, Pople JA, Binkley JS (1984) J Chem Phys 80:3265
20. Jones RO, Lichtenstein AI, Hutter J (1997) J Chem Phys 106:4566
21. Wheeler SE, Sattelmeyer KW, Schleyer PVR, Schaefer III HF (2004) J Chem Phys 120:4683
22. de Visser SP, Alpert Y, Danovich D, Shaik S (2000) J Phys Chem A 104:11223
23. Noury S, Krokidis X, Fuster F, Silvi B (1997) TopMoD package
24. Kohout M, Savin A (1996) Int J Quant Chem 60:875
25. Silvi B (2004) Phys Chem Chem Phys 6:656
26. Silvi B (2003) J Phys Chem A 107:3081
27. Noury S, Colonna F, Silvi B (1998) J Mol Struct 450:59
28. McWeeny R (1992) Methods of molecular quantum mechanics. Academic, London
29. Bader RFW (1975) In: Chalvet O, Daudel R, Diner S, Malrieu JP (eds) Localization and delocalization in quantum chemistry, vol I. Reidel, Dordrecht, pp 15–38
30. Savin A, Silvi B, Colonna F (1996) Can J Chem 74:1088
31. Krokidis X, Silvi B, Alikhani ME (1998) Chem Phys Lett 292:35
32. Berski S, Andrés J, Silvi B, Domingo LR (2003) J Phys Chem A 107:6014
33. del CarmenMichelini M, Sicilia E, Russo N, Alikhani ME, Silvi B (2003) J Phys Chem A 107:4862
34. Pilme J, Silvi B, Alikhani ME (2003) J Phys Chem A 107:4506
35. Rousseau R, Marx D (2000) Chem Eur J 16:2982
36. McAdon MH, Goddard III WA (1988) J Phys Chem 92:1352
37. Shaik SS, Hiberty PC (1985): J Am Chem Soc 107:3089
38. Maynau D, Malrieu J-P (1988) J Chem Phys 88:3163